Colloids and Surfaces B: Biointerfaces 171 (2018) 368–376

Contents lists available at ScienceDirect

Colloids and Surfaces B: Biointerfaces

journal homepage: www.elsevier.com/locate/colsurfb

Phase behavior of DSPC/$PEG_{40}St$ mixtures at higher emulsifier contents

Sevgi Kilic*, Elif Seniz Bolukcu

Chemical Engineering Department, Izmir Institute of Technology, Urla 35430 Izmir, Turkey

ARTICLE INFO

Keywords:
Microbubble
Stability
Phospholipids
Emulsifier
DSPC
$PEG_{40}St$
Conformational change
Langmuir monolayer
Ultrasound contrast agent

ABSTRACT

Phase behaviors of 1,2-Distearoyl-sn-glycero-3-phosphocholine (DSPC) and polyoxyethylene(40)stearate ($PEG_{40}St$) were investigated with Langmuir monolayer isotherms and Brewster angle microscopy (BAM) imaging at DSPC/$PEG_{40}St$ molar ratios ranging from 9:1 to 5:5. Two plateaus were found in the Langmuir isotherms which were relatively shorter for the 9:1 mixture and extended significantly by increasing the $PEG_{40}St$ content, indicating that the $PEG_{40}St$ squeezed out whereas more emulsifier retained in the monolayer at higher $PEG_{40}St$ contents. A strong hysteresis was observed when the mixed monolayers were subjected to compression-expansion cycles. The degree of hysteresis for the first cycles also increased with increasing $PEG_{40}St$ content in the monolayer. Gray scale intensities in the Brewster angle microscopy images were determined for pure DSPC and pure $PEG_{40}St$ and a scale was established to better interpret the morphologies for the mixtures. Bud and vessels formed during the $PEG_{40}St$ squeezed out upon compression. Upon expansion, $PEG_{40}St$ and DSPC is reappeared on the monolayer. When considered BAM images together with the Langmuir isotherm, $PEG_{40}St$ molecules were found to be well distributed within the DSPC molecules at lower DSPC/$PEG_{40}St$ mole ratios and mostly phase separated at higher mole ratios. It was concluded that higher $PEG_{40}St$ content would be advantageous for the design of an efficient and cheaper ultrasound contrast agents.

1. Introduction

Ultrasound is a diagnostic imaging modality widely used in medicine because it is non-invasive, low risk, low cost, and portable technique providing real-time imaging [1]. However, it suffers from poor image quality because blood, healthy liver, spleen and kidney have similar acoustic properties [2]. The image quality can be improved using microbubbles as ultrasound contrast agents [3]. However, low stability of the microbubbles limits their use for extended period of time in clinical settings. There are mainly two components playing major role in microbubble stability, namely, gas core and the shell [4]. Use of gases with low blood dissolution relatively improved the microbubble stability; however, the shell needs to be redesigned for more stable and effective microbubbles [4].

The shell of a microbubble can be biocompatible protein, polymer, or lipid [1]. Previous studies showed that microbubbles coated with protein and polymer shells demonstrated gas loss due to formation of cracks on the shell under ultrasonic pulses. Additionally, protein coated microbubbles tend to adhere into vasculature [1,5]. On the other hand, lipid coated microbubbles were found highly echogenic due to their soft shells resulting from weak intra-lipid interactions [2,6–9]. It is well-understood that phospholipids form liposomes [10,11]. Addition of emulsifiers can transform the bilayers into a monolayer as in microbubbles [12–15]. Tween-40, lipopolymers such as DSPE-PEG_{5000}, DSPE-PEG_{2000}, and Polyoxyethylene-40-stearate ($PEG_{40}St$) were used as emulsifier in microbubble formulations [16–22]. The large size of the hydrophilic polar headgroups of the polyethyleneoxide (PEG) chain leads the emulsifier to acquire a more cone-shape conformation causing the bilayers to convert into monolayers [23]. Hence, phospholipids together with the emulsifiers can form a monolayer around the gas bubbles.

Not all lipids are miscible with emulsifiers [11]. For instance, it was shown that emulsifier is only miscible with expanded phase lipids with carbon number of the acyl chain less than 16 but not with condensed phase lipids [11,19]. Immiscibility of the emulsifier with the condensed phase lipid was attributed to the bulkiness of the PEG-chains of the emulsifier [4]. It appears that stable microbubbles can be produced if gas bubbles are stabilized by the condensed phase lipids with sufficient amount of the emulsifier to form a condensed/cohesive layer around the gas bubble.

A lipid-to-emulsifier mole ratio of 9:1 is generally used for the microbubble composition [4,18,20,24–28]. The phase formation, miscibility, and microbubble stability of this composition have still been under investigation. Emulsifier content less than 10% (9:1 mixture) is

* Corresponding author.
E-mail address: sevgikilic@iyte.edu.tr (S. Kilic).

https://doi.org/10.1016/j.colsurfb.2018.07.046
Received 8 May 2018; Received in revised form 23 June 2018; Accepted 23 July 2018
Available online 24 July 2018

however small to reveal the effect of emulsifier on the phase behavior of the lipid-emulsifier mixtures because the majority of the shell component, more than 90%, is composed of lipids alone. Therefore, higher emulsifier contents are needed to gain more significant information about the effect of the emulsifier on the monolayer cohesiveness. To the best of our knowledge, the phase behavior of DSPC/$PEG_{40}St$ mixture with more than 15% of the emulsifier [11] have not been reported in the current literature.

In the present work, DSPC/$PEG_{40}St$ mixtures in a range from 9:1 to 5:5 mol ratios were prepared and their miscibility were investigated using surface pressure-area isotherms coupled with the Brewster angle microscopy (BAM) imaging. Two plateaus were found in the Langmuir isotherms indicating the squeeze out of the $PEG_{40}St$ molecules from the monolayer. Plateaus were relatively shorter for the 9:1 mixture and extended significantly by increasing the $PEG_{40}St$ content. In our recent paper, we developed a quantification method to estimate the squeeze out amount of $PEG_{40}St$ from Langmuir isotherms [29]. Almost 93%, 82%, and 53% of PEG40 St displaced for the 9:1, 7:3, and 5:5 mixtures, respectively, at the end of the first collapse plateau [29]. Remaining $PEG_{40}St$ squeezed out at the end of the second collapse plateau, where 20% of $PEG_{40}St$ still contained within the 5:5 composition [29]. Here, a scale was established on the Brewster angle microscopy (BAM) images of the monolayers to better interpret the morphologies of the mixtures. It was shown that $PEG_{40}St$ molecules were well distributed within the DSPC molecules at lower DSPC/$PEG_{40}St$ mole ratios and mostly phase separated at higher mole ratios. Compression-expansion cycles up to surface pressures below and above the collapse plateaus showed a solid monolayer at the higher surface pressures and produced cracks during expansions. These cracks were bare sub phase. It was concluded that increasing $PEG_{40}St$ content would be advantageous to design more stable lipid based microbubbles and reduce the cost for the ultrasound contrast agents.

2. Materials and methods

2.1. Materials

1,2 Distearoyl-sn-glycero-3-phoshhocholine (DSPC, 99%) and Polyoxyethylene-40- stearate ($PEG_{40}St$) were purchased from Sigma Aldrich (St. Louis, MO). Chloroform ($CHCl_3$, 99.4%) was purchased from Merck and used as a solvent to prepare spreading solutions. Ultrapure water used as sub phase was produced by Millipore purification system with specific resistivity of 18 MΩ cm. The required amounts of DSPC (MW, 790.16 g/mole) and $PEG_{40}St$ (MW, 2044 g/mole) were calculated for the 9:1; 8:2; 7:3; 6:4 and 5:5 M ratios of the mixtures and dissolved in chloroform so that the resulting final solid concentration was 0.7 mg/ml. After chloroform addition, the vials were immediately sealed with screw cap to avoid chloroform evaporation and kept in the freezer at -22 °C. The sealed vials were homogenized using a bath sonicator before spreading the solution at the air-water interface and warmed up to the room temperature under continuous stirring with the cap closed. About 30 to 50 µl of solution was spread over the water subphase to reach the desired initial mean molecular area.

2.2. Langmuir monolayer isotherms

The experimental procedure for the Langmuir isotherms of the monolayers was reported in our previous paper [29]. Briefly, Langmuir-Blodgett system (KSV minitrough, Finland) with two movable teflon barriers was employed to study the phase behavior of the binary systems and their pure components. The system was enclosed in a plexyglass box to minimize possible contamination of air-monolayer-water interface and the disturbance of the monolayer by the air currents. The Langmuir trough was filled with ultrapure water with specific resistivity of 18 MΩ cm produced by a Millipore purification system. Cleanness of the air-water interface was confirmed by closing and opening the barriers on the pure water and ensuring that surface pressure readings do not differ by more than ± 0.1 mN/m. The lipid solutions were spread on the water subphase via Hamilton micro syringe. The chloroform was allowed to dry for 20 min to obtain monolayers at the air-water interface. The surface pressure-area (π-A) isotherms were obtained via symmetric compression of the monolayers by the two barriers. A compression speed of 5 mm/min was used in all experiments. Each isotherm was performed 4–5 times to ensure reproducibility of the isotherms.

The cycle experiments of the isotherms were carried out by periodic compression followed by an expansion. For these experiments, a monolayer was compressed until the surface pressure reached the targeted pressure of either 30 mN/m or 50 mN/m, then the monolayer was allowed to equilibrate for 20 min and expanded to the initial pressure while the surface pressure was maintained constant. After allowing 20 min to equilibrate, the subsequent compression and expansion cycles were performed.

2.3. Brewster angle microscopy (BAM) images of the monolayers

Morphology of the monolayers were investigated by Brewster Angle Microscope (KSV Optrel BAM300) mounted on the Langmuir trough (KSV minitrough, Finland). Standard HeNe laser was used as the light source emitting linearly p-polarized light with an intensity of 10 mW at a wavelength of 632.8 nm. High quality Glan-Thompson polarizers were used with the polarization ratio of 10^{-6}. The images of the monolayers were captured by the CCD digital monochrome video camera (EHD®kamPro02) attached to the instrument with a resolution of 768 × 494 pixels. The images were acquired using an objective (Mitutoyo, Japan) with 10× magnification (WD: 33.5 mm, NA: 0.28, FOV: 400 × 300 µm).

For the BAM images, the microscope was firstly adjusted to the incident beam fixed at Brewster angle of water (53°) for no reflection from the surface, resulting in completely dark background. After spreading the monolayer, reflected lights from the monolayer surface passing through a second polarizer were recorded with the CCD camera for the same settings. Experiments were carried out at 22 ± 1 °C using circulating water bath. The BAM images of the samples were stored digitally at every 30 s. Representative images were selected for evaluations. The gray scale intensity of the images were determined using the ZEN® software (Carl Zeiss, Germany).

3. Results and discussion

The miscibility behaviors of DSPC and $PEG_{40}St$ mixtures were investigated at molar ratios of DSPC/$PEG_{40}St$ ranging from 9:1 to 5:5. Fig. 1a shows the surface pressure (π)-mean molecular area isotherms for pure DSPC, pure $PEG_{40}St$, and DSPC/$PEG_{40}St$ binary mixtures at different molar ratios, as also reported in our previous paper [29]. The discontinuities as the main turning points for the mixed monolayer isotherms and the locations of the isotherms in the low and high compressibility regions were shown separately in Fig. 1b for the 8:2 mixture as an example. Fig. 1c shows the compression modulus (C_s^{-1}) for the pure components and 8:2 mixture in particular as an example, which was used to detect phase transitions [30,31]. The compression modulus is defined by Eq. (1) [30,32,33]

$$C_s^{-1} = -A\frac{(d\pi)}{(dA)} \quad (1)$$

where A is mean molecular area at that particular surface pressure. As seen in Fig. 1a and b, pure DSPC monolayer demonstrated liquid-condensed (LC) phase at the air-water interface at room temperature due to strong cohesive interactions between C_{18} aliphatic chains [32,34,35]. From the compression modulus, as shown in Fig. 1c, the collapse pressure for DSPC was found to be about 59 mN/m, at which C_s^{-1}

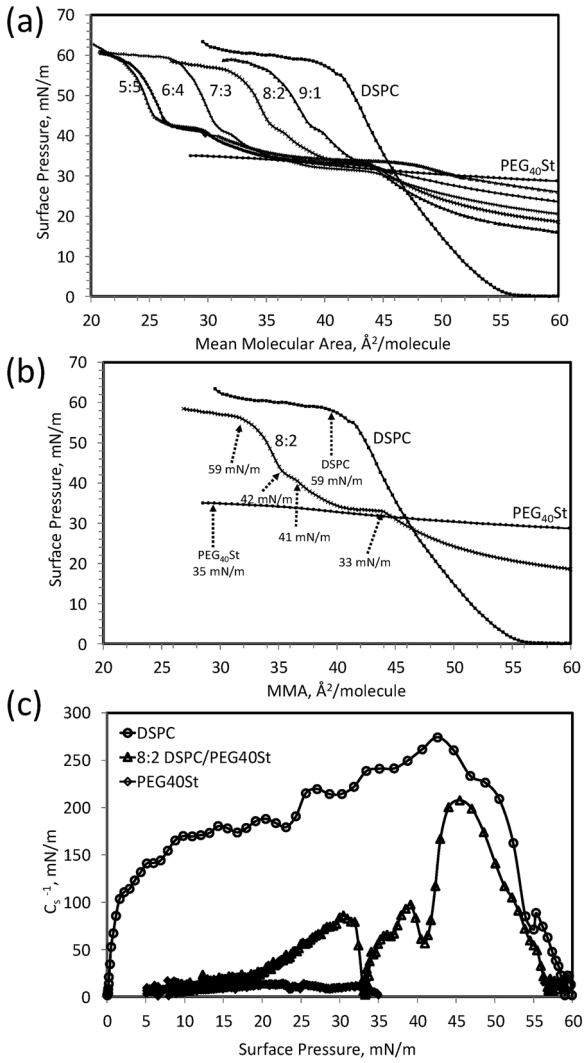

Fig. 1. Surface pressure-mean molecular area isotherms of (a) DSPC, $PEG_{40}St$, and their mixed monolayers at different mole ratios, (b) typical discontinuities as the turning points indicated by the arrows, (c) compression modulus (C_s^{-1}) for pure DSPC, pure $PEG_{40}St$, and 8:2 mixture of DSPC/$PEG_{40}St$.

showed a minimum, at which, as shown in Fig. 1b, the mean molecular area for DSPC was found to be about 40 Å^2/molecule, being in good agreement with the literature [36–38]. Unlike DSPC, pure $PEG_{40}St$ monolayer exhibited a non-zero surface pressure even at very low molecular densities. As shown in Fig. 1c, at which C_s^{-1} showed a minimum, the collapse pressure for $PEG_{40}St$ was found to be 35 mN/m, consistent with the literature [36,39]. However, there are inconsistencies about the mean molecular area of $PEG_{40}St$ in the literature such that the mean molecular area for the $PEG_{40}St$ were reported to be 40 Å^2/molecule [40], 30 Å^2/molecule [41], and 20 Å^2/molecule [16] at its collapse pressure. Here, our measurements showed in Fig. 1b that the mean molecular area for $PEG_{40}St$ is about 30 Å^2/molecule at its collapse pressure of 35 mN/m. Pure $PEG_{40}St$ did not result in sharp increase in the surface pressure and remained in the expanded phase until its collapse pressure.

The mixture isotherms were measured to be located between the isotherms of the pure DSPC and pure $PEG_{40}St$ components. As shown in Fig. 1c, discontinuities were identified on the mixture isotherms. The first plateau initiated at 33 mN/m, which was below the collapse pressure of pure $PEG_{40}St$. A second discontinuity was seen for the mixtures at the surface pressure of about 41 mN/m, which was the end of the first collapse plateau and start of the second plateau. The second collapse plateau ended at the surface pressure of about 42 mN/m, which slightly increased from 42.4 mN/m to 44.7 mN/m with increasing emulsifier content for the mixtures [29]. The last discontinuity was at the surface pressure of about 59 mN/m for the mixtures, which were interestingly intersected with the collapse pressure of DSPC. At each discontinuity, as shown in Fig. 1a, the mean molecular area decreased with increasing emulsifier content for the mixtures. The decrease in the mean molecular area indicated that there are either considerable changes in the conformation of the PEG-chain of the emulsifier or squeeze out of $PEG_{40}St$ from the monolayer [4,11,29]. The squeeze out amount of $PEG_{40}St$ was quantified in our previous paper [29] and found that almost all $PEG_{40}St$ were lost from the monolayer at the last discontinuity region so that the collapse pressures for the mixtures were the same with the collapse pressure for DSPC alone. The changes became more significant and clearly visible as the emulsifier contents were increased in the mixture.

The mixture isotherms demonstrated more expanded behavior with increasing $PEG_{40}St$ content in the monolayer below the collapse pressure of the emulsifier, which is due to the bulky polymer chains spread at the interface. However, above the plateau, the isotherms shifted to the smaller mean molecular areas with increasing emulsifier content. It was reported earlier that the location of the DSPC/$PEG_{40}St$ mixture isotherms up to 15% of $PEG_{40}St$ content was independent of the emulsifier content after the plateau region, exhibiting an isotherm identical to that of pure DSPC [11]. However, we observed that the isotherms were located at more left of DSPC with increasing emulsifier content, as also observed with DSPC/DSPE-PEG_{2000}, DPPC/PEG_8St and Span60/$PEG_{40}St$ mixtures [33,35,41,42]. Our mixture isotherms displayed plateaus broadening with increasing $PEG_{40}St$ content in the monolayer. Enlargement of the plateau was also observed in DSPC/$PEG_{40}St$ monolayers elsewhere with $PEG_{40}St$ content up to 15 mol% [11], whereas the isotherms of the Span60/$PEG_{40}St$ mixed monolayers were seen to be intersecting at a point above the plateau region [41]. With further compression of the monolayer, additional smaller plateaus were observed at surface pressure of about 41 mN/m for all mixed monolayers. Similar to the first plateau, mixtures displayed more prominent plateaus with increasing $PEG_{40}St$ content. The increase in the extent of second plateau was also seen in Span60/$PEG_{40}St$ mixtures, exhibiting a decrease in the starting surface pressure of the plateaus from 45 mN/m to 38 mN/m with increasing molar fraction of $PEG_{40}St$ in the monolayer [41]. The second plateau was attributed to a partial removal of the emulsifier from the mixed monolayers [41]. The length of the plateaus clearly signifies that the amount of the emulsifier retained in the monolayer is proportional with the emulsifier content. We evaluated the squeeze out amount of $PEG_{40}St$ from Langmuir isotherms in our previous paper [29]. Almost 93%, 82%, and 53% of PEG40 St displaced for the 9:1, 7:3, and 5:5 mixtures, respectively, at the end of the first collapse plateau [29]. The remained $PEG_{40}St$ squeezed out at the end of the second collapse plateau of about 42 mN/m, except 20% of $PEG_{40}St$ still remained with the 5:5 composition [29]. The lack of the second plateaus in the previous study for the DSPC/$PEG_{40}St$ mixtures up to 15% of the emulsifier [11] were probably due to the onset of buckling in the monolayer resulting from the different amount of the material spread initially at the air-water interface [43] and/or the insufficient amount of the emulsifier to observe the changes.

Compression-expansion cycles of the Langmuir monolayers were investigated to understand the $PEG_{40}St$ squeeze out from the monolayers and to evaluate how well the monolayer components can retain their configuration during the expansion after a compression [40,44]. Fig. 2 shows the compression-expansion cycles of DSPC/$PEG_{40}St$ mixed monolayers for 9:1, 7:3 and 5:5 mixtures for comparison. Surface pressures of 30 mN/m and 50 mN/m were selected as the pressures below and above the collapse pressures of the mixtures. The monolayers were compressed to either the surface pressures of 30 mN/m or 50 mN/m, held at that pressure for 20 min, and then expanded to the low surface pressure, allowing 20 min to equilibrate before the

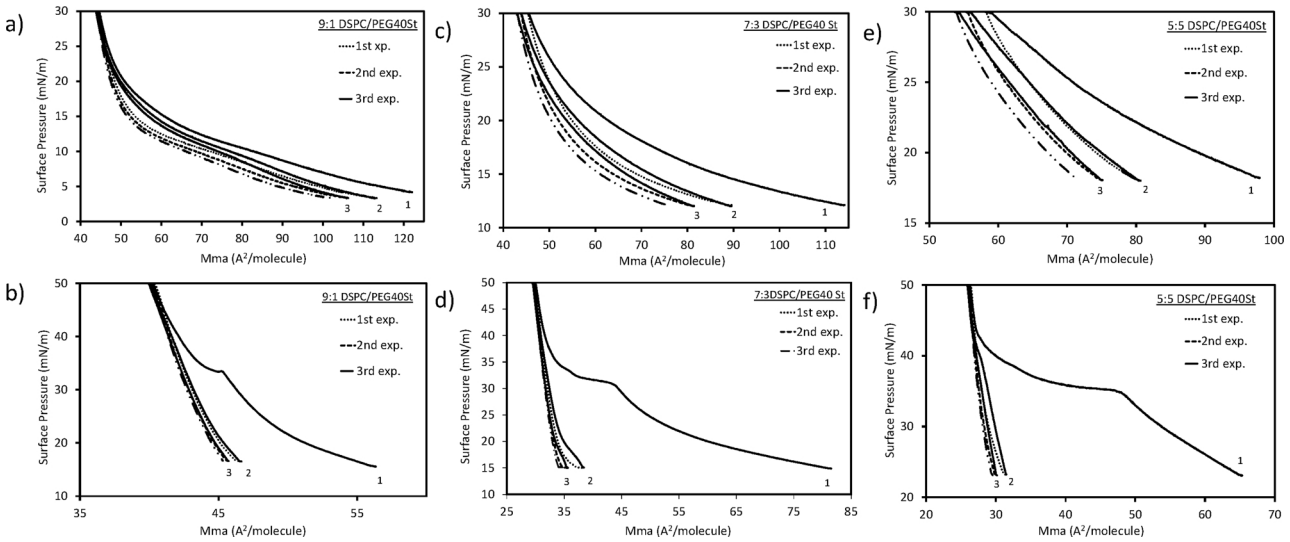

Fig. 2. Compression-expansion cycles of (a,b) 9:1, (c,d) 7:3, (e,f) 5:5 DSPC/$PEG_{40}St$ mixed monolayers compressed up to a surface pressure of 30 mN/m (a, c, e) and 50 mN/m (b, d, f). Solid lines with numbers indicate the corresponding compression isotherm in the cycle.

subsequent compressions. As shown in the figure, when the mixed monolayers were compressed to the target pressure of 30 mN/m (Fig. 2a, c, e), the expansion curves did not return to the starting point of the preceding compression curves, indicating a hysteresis. The magnitude of hysteresis scaled with the mol% of $PEG_{40}St$ in the mixture. In a separate study, the Langmuir isotherms of pure DSPC did not show a significant change during successive compression-expansion cycles while pure $PEG_{40}St$ demonstrated very large shifts to the lower mean molecular areas in each cycle (data not shown). Therefore, this hysteresis was attributed to conformational changes in the PEG-chains since the emulsifier was considered not to be lost to the subphase when the monolayer compressed to 30 mN/m, which is below the collapse pressure of 33 mN/m for the mixtures [11,40].

When the mixed monolayers were subjected to compression-expansion cycles to the target pressure of 50 mN/m, a strong hysteresis was observed in the first compression-expansion cycle (Fig. 2b, d, f). The other two subsequent cycles did not produce significant hysteresis. The degree of hysteresis for the first cycles increased with increasing $PEG_{40}St$ content in the monolayer. A very small plateau was observed at about 40 mN/m in the second compression cycle for the 5:5 mixture. The second plateaus were not observed for the other isotherms when high amount of material was spread at the interface [43]. The mean molecular areas were the same at the end of each compression to 50 mN/m for all mixtures indicating the formation of DSPC-rich monolayer and a significant amount of $PEG_{40}St$ squeeze out from the monolayer after the first compression.

The morphology and miscibility behaviors of DSPC and $PEG_{40}St$ were investigated by the Brewster angle microscopy (BAM). Fig. 3a shows the selected BAM images among the images subsequently taken at 30 s intervals during compression for pure DSPC and pure $PEG_{40}St$. The BAM image for pure DSPC showed a fractured bright surface floating on the water subphase at the initial spreading conditions, where it did not exert a surface pressure. With moving barriers towards each other, a continuous monolayer of DSPC formed when the DSPC layer was compressed to higher surface pressures. During compression, the level of the air/water interphase elevated so that the focus on the images moved to the bottom of the images taken by the camera at a fixed distance position. A continuous dark BAM image was obtained for the pure $PEG_{40}St$ at the initial spreading pressure of 11.66 mN/m. Upon compression, the images became brighter. It was reported that the intensity in the BAM images depends on the film thickness and film optical properties [45–48]. Therefore, gray scale intensities were determined along the images using ZEN® image processing software. Fig. 3b shows the brightness levels obtained for the pure DSPC and pure $PEG_{40}St$ monolayers. The film thicknesses were not calculated because generally the refractive indices for these films thinner than 20 nm could not be accurately determined [49,50]. At the initial spreading pressure of DSPC, the water subphase produced a completely dark image with a "zero" gray scale intensity on a line at the focus area of the BAM image as shown in the figure. The continuous monolayer of the DSPC produced totally bright image with a higher gray scale intensity value. The fractured domains produced gray scale intensities in between these two intensity levels. The mid-level intensities indicated that some of the DSPC molecules freely floating on the surface are tilted on the subphase [46] at the air-water interface so that their film thickness is relatively smaller.

The gray scale intensity value was very low for the BAM image of $PEG_{40}St$ at its initial spreading pressure. However, the gray scale intensities increased with compression of $PEG_{40}St$ monolayer as the surface pressure was increased up to its collapse pressure of 35 mN/m. The increase in the gray scale intensity can be attributed to the conformational changes in the PEG-chains [44] as illustrated at the inset of Fig. 3b for the $PEG_{40}St$ gray scale intensity. It is well established with the Alexander-de Gennes theory that when PEG-grafted surfactants are spread at the air-water interface, the hydrophilic headgroups acquire different conformations at the interface [44]. At very low densities, PEG headgroups spread at the interface with a "pancake" conformation. Repulsive interactions between the polymer chains start when the distance between the polymer chains is comparable to the Flory radius (R_F) given by $R_F = a.N^{3/5}$ where a is monomer size (equal to 0.35 nm for PEG) and N is the number of ethyleneoxide monomer units [44]. When the polymer chains approach a distance comparable to Flory radius, they begin to extend into a third dimension towards the water phase called "mushroom" to "extended mashroom" conformations, due to steric repulsion between the hydrophilic polymer chains. At a distance smaller than the Flory radius, the chains extend into subphase, leading to formation of "brush-like" conformation [44]. Therefore, a scale was established for the interpretation of the conformational changes of DSPC and $PEG_{40}St$ in the mixtures at different compression levels.

The brightness intensities obtained from the examination of the BAM images for pure DSPC and pure $PEG_{40}St$ were divided into four levels. The zero intensity level (L-0) corresponds to the water subphase since there is not any lipid or emulsifier molecules at the air-water interface. The first level of the gray scale intensity, L-1, was assigned to the pancake conformation of $PEG_{40}St$ at very low spreading surface pressures. The gray scale intensity level increases with the increase in

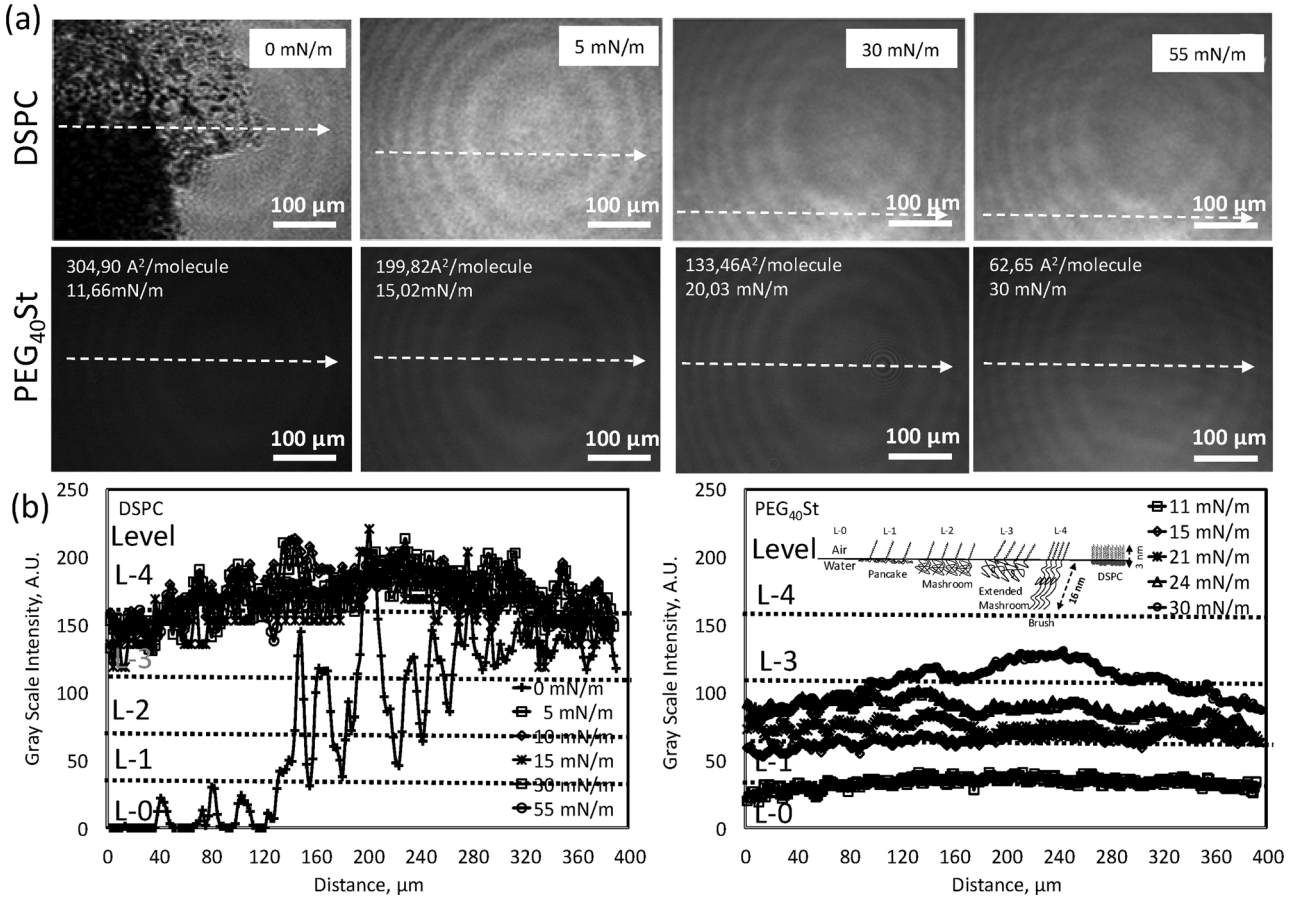

Fig. 3. (a) BAM images of pure DSPC and pure $PEG_{40}St$ monolayers at different compressions (b) Gray scale intensity levels for DSPC and $PEG_{40}St$ at different surface pressures. Inset is the possible conformations of the PEG-chains.

the degree of its condensation at higher surface pressures. Therefore, the L-2 to L-3 levels were assigned to the mushroom and extended mushroom conformations of the PEG-chains. The brush conformation of the $PEG_{40}St$, if occurs, appear in the L-4 level in the scale. Considering the length for the C—C bond to be about 1.53 Å [46], the chain length for the DSPC and $PEG_{40}St$ hydrocarbon tails would be about 2.75 nm since they both have 18-carbons on their hydrocarbon tails. Assuming the projected length for each ethylene oxide monomer, —(CH_2—CH_2—O)—, to be 3.7 Å [42], the length of 40 PEG-chains would be about 16.6 nm at its brush conformation. Hence, the film thickness for the DSPC and $PEG_{40}St$ in its brush conformation would be about 3 nm and 19 nm, respectively [26,51], where the film thickness for the $PEG_{40}St$ would be about 6 times greater than the film thickness for the DSPC. Hence, the gray scale intensity would be expected to be much higher for the $PEG_{40}St$ at its brush conformation than the brightness level for the condensed DSPC monolayer. However, the $PEG_{40}St$ rarely form a condensed brush layer [51–53] and therefore, the gray scale intensity became usually lower for the PEGylated emulsifier compared to the condensed DSPC molecules. Therefore, in the scale, the bright-end of the gray scale intensity level indicates mainly the conformation for the DSPC-rich monolayer and the dark-end of the gray scale intensity level indicates the conformation of the PEG-chains of the $PEG_{40}St$, which depends on their chain length and packing density [12,14].

Fig. 4 shows the BAM images of DSPC/$PEG_{40}St$ mixtures from 9:1 to 5:5 M ratios captured at the surface pressure of 25 mN/m during the continuous compression. The measured mean molecular areas of the mixtures were also indicated on each image. These monolayers were in the high-to-moderate compressibility region and the mean molecular areas of the mixtures increased with increasing emulsifier content at the constant surface pressure of 25 mN/m. The mean molecular area of the pure DSPC was measured to be about 47.5 $Å^2$/molecule at the surface pressure of 25 mN/m (Fig. 1). Because the DSPC molecules are in liquid-condensed state, its mean molecular area can be considered not significantly varying in these different mixtures at the specified surface pressure. Therefore, the relatively more rigid DSPC molecules can be employed as the reporter molecule to estimate the mean molecular areas occupied by the $PEG_{40}St$ molecules in the mixtures using the balance equation [29]: $A_{12}=x_1.<A_1>+x_2.<\boldsymbol{A_2}>$, where A_{12} is the measured mean molecular area for the mixture, x_1 and x_2 are mole fractions of each component, and $<A_1>$ and $<A_2>$ are the mean molecular area for the DSPC and $PEG_{40}St$ occupied in the mixture, respectively, at the specified surface pressure. Knowing x_1, x_2 for the DSPC and $PEG_{40}St$ compositions and, assuming that the DSPC molecules are rigid enough where its mean molecular area does not change significantly with the small deviations in the surface pressures, the mean molecular area for DSPC ($<A_1>$) is approximately the same with its ideal mean molecular area (A_1) obtained from the pure DSPC isotherm, the mean molecular area for the $PEG_{40}St$ ($<A_2>$) can be calculated in the mixtures as shown in Fig. 5. This method to estimate the mean molecular area of $PEG_{40}St$ in DSPC is the first, to the best of our knowledge, reported in the literature [29]. As seen, surprisingly, the calculated mean molecular area for $PEG_{40}St$ was about 42 and 55 $Å^2$/molecule for the 9:1 and 8:2 DSPC/$PEG_{40}St$ mole ratios, respectively, which were almost the same with the mean molecular area of 47.5 $Å^2$/molecule for the DSPC at lower emulsifier mole ratios. Larger mean molecular areas were obtained for the higher emulsifier mole ratios, for which the mean molecular areas for $PEG_{40}St$ were 69 and 86 $Å^2$/molecule for the 7:3 and 5:5 DSPC/$PEG_{40}St$ mole ratios, respectively. The mean molecular area for the $PEG_{40}St$ molecules was

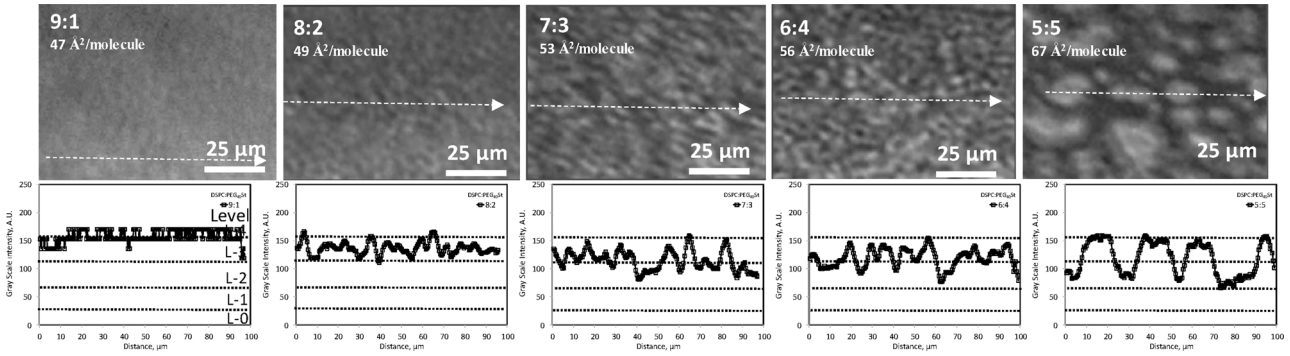

Fig. 4. BAM images of pure DSPC and DSPC/$PEG_{40}St$ mixed monolayers at the air-water interface captured at surface pressure of around 25 mN/m during compression.

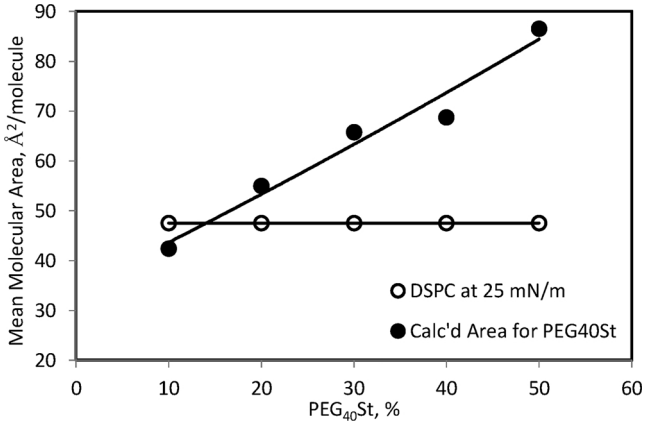

Fig. 5. Mean molecular areas calculated for $PEG_{40}St$ in the mixtures.

more than double for the 5:5 mixture compared to that for the 9:1 mixture. The mean molecular area for the pure $PEG_{40}St$ was measured to be about 91.5 $Å^2$/molecule at this compression level for the surface pressure of 25 mN/m. It is understood that $PEG_{40}St$ molecules were well distributed within the DSPC molecules at lower mole ratios and phase separated at higher mole ratios. The well-distributed $PEG_{40}St$ molecules were compressed by the DSPC molecules at the molecular level pushing the PEG-chains down underneath the monolayer to form an extended mushroom conformation at lower DSPC/$PEG_{40}St$ mole ratios since the $PEG_{40}St$ concentration was only 10% in the 9:1 mixture and the majority of the composition was composed of the DSPC molecules. At higher DSPC/$PEG_{40}St$ mole ratios, the $PEG_{40}St$ molecules seem to be phase separated and demonstrate predominantly a PEG-PEG compression so that the mean molecular area is relatively higher, indicating a mushroom conformation.

The BAM images for the DSPC/$PEG_{40}St$ mixed monolayers from 9:1 to 5:5 M ratios demonstrated bright domains on relatively dark background. The bright domains indicated the condensed DSPC-rich monolayer and less bright background indicated the $PEG_{40}St$-rich monolayer. These domains are noncircular due to anisotropic and unidirectional compressions [54]. As shown in the figure, the size of the expanded phases increased with the emulsifier content and considerably phase separated at the 5:5 mol ratio. The gray scale intensity for the dark-end relatively decreased as the $PEG_{40}St$ content was increased in the mixtures, indicating that the $PEG_{40}St$ in mushroom conformation at the 5:5 mol ratio converted into the extended mushroom to brush conformation towards the 9:1 DSPC/$PEG_{40}St$ mole ratio. The gray scale intensity level for the bright-end intensity was higher for the 9:1 mol ratio and decreased slightly with increasing the $PEG_{40}St$ content, demonstrating a lower film thickness and/or less condensed monolayer compared to the more condensed pure DSPC monolayers. At constant surface pressure, with increasing amount of the emulsifier, the distance between PEG-chains decreased, promoting the conformational changes for which the cohesive interactions between aliphatic chains weakened due to an increase in the distance between DSPC molecules favoring the conformational changes by anchoring the molecules to the interface. Therefore, the increase in the size of the condensed domains at higher molar ratios, despite the decrease in DSPC mole ratio, implies that some of the emulsifier molecules were incorporated into DSPC matrix through conformational changes, while the excess emulsifier molecules in the mixtures partitioned out of the condensed phase, resulting in DSPC-enriched and liquid expanded (LE) $PEG_{40}St$-enriched domains.

Morphological changes in the mixed monolayers were analyzed during compression-expansion cycles. Fig. 6 shows the BAM images of the 9:1 and 5:5 mixed monolayers compressed to 30 mN/m below the collapse pressure of the mixture and then expanded to 8 mN/m and 12 mN/m for three cycles, respectively, which were the minimum surface pressures that the trough area allowed. As seen from Fig. 6a, at 8 mN/m surface pressure before the first compression, 9:1 mixture displayed initially bright spots connected through less condensed phases spread with relatively dark background. The gray scale intensity at the low-end indicated that the $PEG_{40}St$ was in mushroom conformation although its content was only 10% while the majority was the DSPC in the monolayer. The brightness level at the high-end indicated the DSPC-rich condensed domains forming bright spots at the air-water interface. The BAM images of the monolayer at surface pressure of 30 mN/m revealed that the condensed phases became more interlinked during the compression with the fusion of less condensed/fluid regions to form extended mushroom conformation. Interlinking of the condensed domains with compression was also observed in 9:1 DPPC/$PEG_{40}St$ mixture via fluorescence microscopy [11]. Brightness level at high-end indicated that the DSPC became tilted on the surface when mixed with the $PEG_{40}St$ and formed a relatively thinner monolayer. Upon expansion, the monolayer relaxed without significantly altering their conformations in the subphase as evidenced from the brightness level at high-end. The gray scale intensity at the “zero” level revealed that the dark regions were the bare water. It seems that a solid-like monolayer film formed during compression while a network structure formed during expansion without significant molecular relaxation. Upon compression for the second and third cycles, similar condensed monolayers formed. Bright spots disappeared in the subsequent expansion cycles. The shift of the isotherm to the left is generally interpreted as a material loss during compression-expansion cycles [44]. Considering no material loss from the monolayer prior to collapse pressure of the emulsifier [11], the shifts to a lower mean molecular area in the surface pressure-area isotherm were attributed to the conformational changes in PEG-chains of the emulsifier in each cycle. It is evident from the BAM images that not only the molecular compression but also the domain compression took place in the monolayer during the expansion-compression cycles. The Langmuir

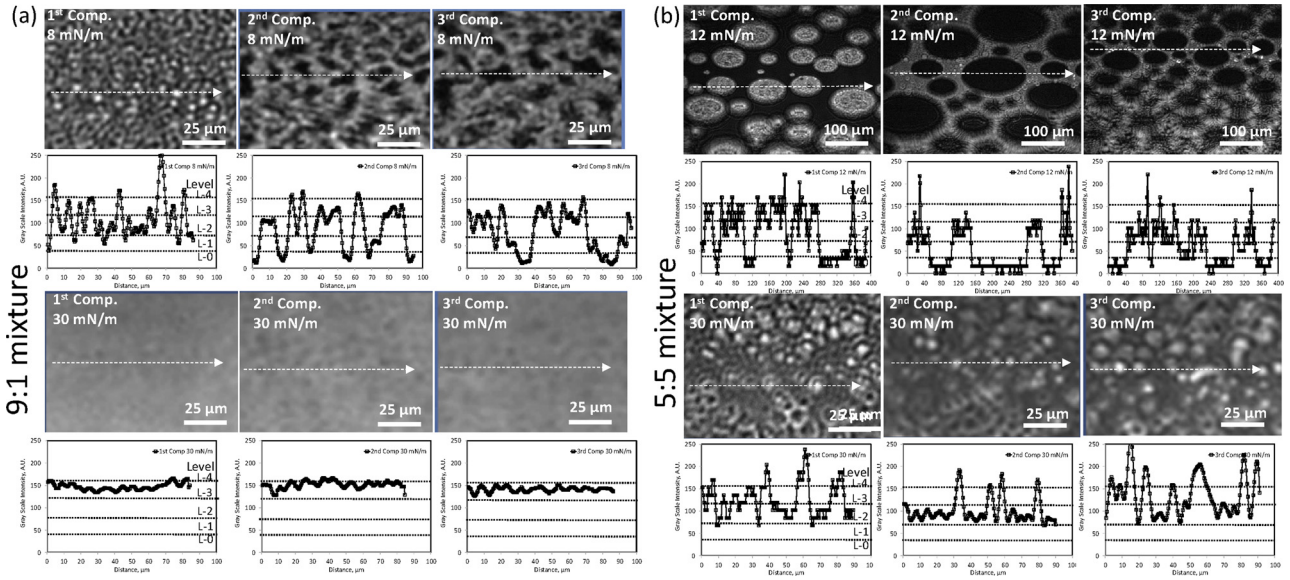

Fig. 6. BAM images of (a) 9:1 (b) 5:5 DSPC/$PEG_{40}St$ mixed monolayers at the air-water interface captured during successive compression-expansion cycles of the monolayer compressed upto surface pressure of 30 mN/m.

isotherms of the compression-expansion cycles also support these observations as the subsequent compression isotherm shifted to the left of the preceding compression isotherm in Fig. 2. It has been reported that PEG-chains in the extended conformation into the subphase bind more water than in random coil conformation [51]. This implies that, as being a hydrophilic polymer, PEG-chains prefer to remain in the extended conformation as their interaction with water is energetically more favorable in the extended state.

As seen in Fig. 6b, 5:5 mixed monolayer initially formed large bright domains within a continuous dark background at the surface pressure of 12 mN/m before the initial compression. The near zero level gray scale intensity indicates that the very large dark phase is the $PEG_{40}St$ in the pancake conformation on the water subphase. The bright domains contained both DSPC and $PEG_{40}St$ mixed monolayers. The gray scale intensity level in these bright domains indicate that at the low-end the PEG-chains show an extended interface-bound mushroom conformation when spread initially at the interface. Upon compression to 30 mN/m, a reduction in size for both the condensed domains and dark background was observed while the number of condensed domains increased. The gray scale intensity for the $PEG_{40}St$ at the low-end indicated that the $PEG_{40}St$ molecules changed conformation from pancake to mushroom conformations. The brightness level at the high-end showed a condensed DSPC-rich islands at the interface. Upon expansion of the monolayer to the lower surface pressure, bright domains become interconnected, forming a continuous network. The zero level gray scale intensity indicated that the dark background was the bare water and the DSPC and $PEG_{40}St$ are mixed in the interconnected network monolayer. However, the brightness level at high-end indicated that the film thickness was lower for the interconnected network. The thinner film was attributed to the tilted or less condensed DSPC molecules [46] upon mixing with the $PEG_{40}St$ molecules in the expanded network. Also, there were bright grains on the monolayer, indicating highly condensed DSPC molecules. Upon recompression, the surface is mostly covered by the $PEG_{40}St$ in mushroom conformation and DSPC was densely packed into islands, circles, and crater-like domains as shown in the figure. The crater-like domains were thought to form from buds, folds, and vesicles [4] filled with water, producing image with relatively lower gray scale intensity within their inner areas. Since no emulsifier is lost to the subphase prior to collapse pressure of the emulsifier [11], interconnection of the bright domains in subsequent cycles implies that there is coexistence of fluid and condensed phases with incorporation of more emulsifier molecules into the condensed regions from the $PEG_{40}St$-rich fluid-phase. These observations are in good agreement with the Langmuir isotherms in the compression-expansion cycles in Fig. 2e showing that the same surface area was achieved for the same surface pressure of 50 mN/m in each cycle.

In the compression-expansion cycle of the monolayers compressed to 50 mN/m, 9:1 mixture was expanded to 14 mN/m (Fig. 7a) and 5:5 mixture expanded to 22 mN/m (Fig. 7b) as the trough area allowed. In the BAM image for the 9:1 mixture, condensed grain-like domains were distributed in a less bright continuous phase. The brightness level at high-end indicated that the bright domains were the condensed DSPC domains and the gray scale intensity level at low-end indicated that the continuous monolayer was $PEG_{40}St$ domains in mushroom conformation. Upon compression to 50 mN/m, a relatively continuous monolayer formed. The Langmuir isotherms indicated a big hysteresis for the first compression-expansion cycle and no hysteresis were seen in the latter two compression-expansion cycles as seen in Fig. 2. The $PEG_{40}St$ molecules were initially in mushroom conformation as evidenced from the gray scale intensity level at low-end and they seemed to squeeze out from the monolayer upon compression to 50 mN/m. The brightness level at high-end at 50 mN/m pressure indicated that a condensed DSPC film formed. The subsequent compression and expansions of 9:1 mixture did not alter the gray scale intensity and produced solid-like monolayer with $PEG_{40}St$ squeeze out. Upon expansion, the monolayer relaxed, however, because the $PEG_{40}St$ content is lower, only 10% in 9:1 mixture, a reinsertion of $PEG_{40}St$ into the monolayer is hardly seen. The relatively low-end gray scale intensity indicate the $PEG_{40}St$ at its extended mushroom conformation, but it could also be defects on the monolayer filled with water showing relatively less-bright regions in the image.

As shown in Fig. 7b, initial spreading of DSPC/$PEG_{40}St$ mixture at 5:5 mol ratio produced continuous monolayer and condensed grain-like domains at the surface pressure of 22 mN/m. Crater-like domains were also produced at the local collapse region occurred on the monolayer [4]. The low-end gray scale intensity indicated the mushroom-like conformation for the $PEG_{40}St$. Upon compression, a slightly rough surface was obtained with small defects on the monolayer [4]. We think that the relatively dark regions are the bud and vessels formed during the $PEG_{40}St$ squeezed out, which attach to the monolayer at its underneath [4,11]. It seems that the bud and vessels filled with water producing relatively lower gray scale intensity levels. Upon expansion,

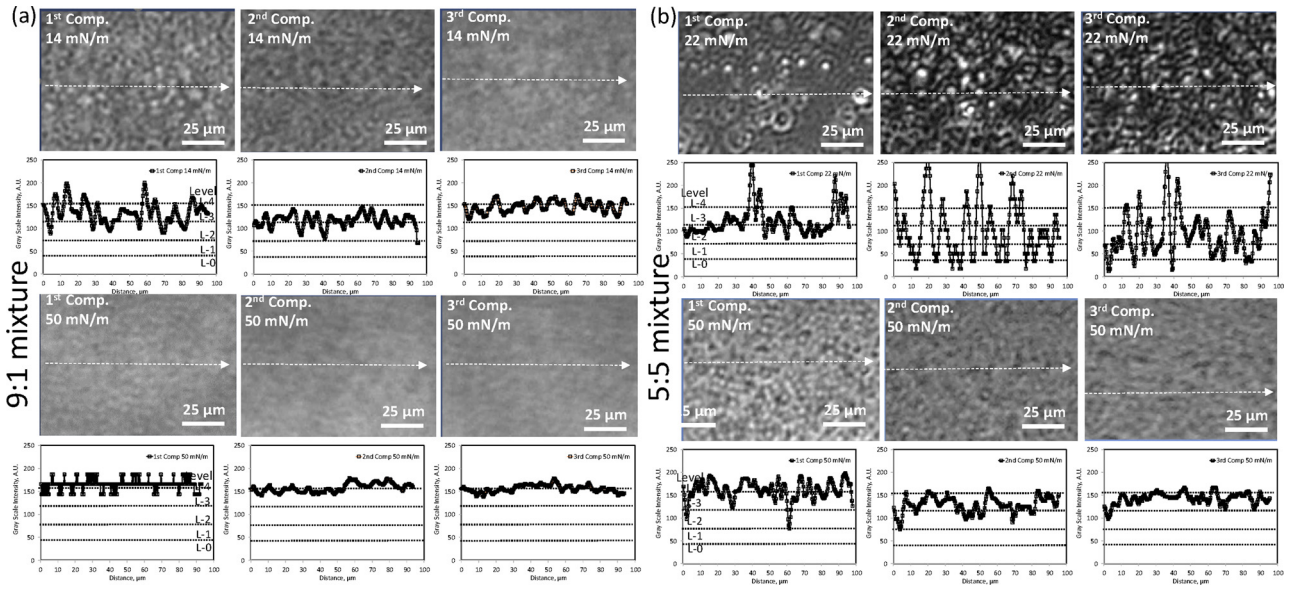

Fig. 7. BAM images of (a) 9:1 (b) 5:5 DSPC/$PEG_{40}St$ mixed monolayer at the air/water interface captured during successive compression-expansion cycle of the monolayer compressed to surface pressure of 50 mN/m.

the bright DSPC islands were reappeared on the film in addition to water subphase as evidenced from the low-end gray scale intensity. $PEG_{40}St$ was also seen from the low-end gray scale intensity to be inserted into the monolayer during expansion [4]. These domains were thicker evidenced from the high-end gray scale intensity, probably due to associations of DSPC and $PEG_{40}St$ molecules. Subsequent compression-expansion cycles produced similar results indicating that the compression of the DSPC/$PEG_{40}St$ monolayer film above the collapse pressure, the $PEG_{40}St$ squeeze out from the monolayer submerged underneath and remained attached to the monolayer [55–57]. Cracks also formed containing water as evidenced from the zero gray scale intensity upon expansion and some of $PEG_{40}St$ reinserted into the monolayer.

4. Conclusions

It is clear that the plateaus on the Langmuir isotherms of the DSPC/$PEG_{40}St$ mixtures with composions less than 9:1 mol ratio is smaller and less sensitive to changes. However, the changes became more significant when the $PEG_{40}St$ mole% was increased. It was understood that $PEG_{40}St$ molecules were well distributed within the DSPC molecules at lower mole ratios, which make the microbubble shell more rigid whereas $PEG_{40}St$ was phase separated at higher mole ratios, making the shell more relaxed. The BAM images and the Langmuir isotherms indicated that the amount of the emulsifier remained in the monolayers is proportional with the emulsifier in the mixture at any compression state. It was concluded that higher $PEG_{40}St$ contents in the monolayer will help to design more stable and persistent lipid based microbubbles used as ultrasound contrast agent and as vehicles in drug delivery systems. Using higher emulsifier content in microbubble formulations would also help decreasing the cost for the ultrasound contrast agents. Considering the cost for DSPC is about $169/g-DSPC [58] and the cost for $PEG_{40}St$ is about $0.22/g-$PEG_{40}St$ [59], the cost for the 5:5 shell composition of DSPC/$PEG_{40}St$ mixture would be much cheaper compared to the customized composition of 9:1 M ratio.

Acknowledgement

We gratefully acknowledge the financial support provided by The Scientific and Technological Research Council of Turkey (TUBITAK) under the Project No. 113M270.

References

[1] S. Hernot, A.L. Klibanov, Microbubbles in ultrasound-triggered drug and gene delivery, Adv. Drug Deliv. Rev. 60 (2008) 1153–1166.
[2] S. Tinkov, R. Bekeredjian, G. Winter, C. Coester, Microbubbles as ultrasound triggered drug carriers, J. Pharm. Sci. 98 (2009) 1935–1961.
[3] E.G. Schutt, D.H. Klein, R.M. Mattrey, J.G. Riess, Injectable microbubbles as contrast agents for diagnostic ultrasound imaging: the key role of perfluorochemicals, Angew. Chem. Int. Ed. 42 (2003) 3218–3235.
[4] J.J. Kwan, M.A. Borden, Lipid monolayer collapse and microbubble stability, Adv. Colloid Interface Sci. 183 (2012) 82–99.
[5] M.A. Borden, D.E. Kruse, C.F. Caskey, S. Zhao, P.A. Dayton, K.W. Ferrara, Influence of lipid shell physicochemical properties on ultrasound-induced microbubble destruction, Ultrason. Ferroelectr. Freq. Control IEEE Trans. 52 (2005) 1992–2002.
[6] K. Kim, C. Kim, Y. Byun, Biostability and biocompatibility of a surface-grafted phospholipid monolayer on a solid substrate, Biomaterials 25 (2004) 33–41.
[7] M.M. Lozano, M.L. Longo, Microbubbles coated with disaturated lipids and DSPE-PEG2000: phase behavior, collapse transitions, and permeability, Langmuir 25 (2009) 3705–3712.
[8] A.L. Klibanov, M.S. Hughes, J.K. Wojdyla, J.H. Wible, G.H. Brandenburger, Destruction of contrast agent microbubbles in the ultrasound field: the fate of the microbubble shell and the importance of the bubble gas content, Acad. Radiol. 9 (2002) S41–S45.
[9] E.C. Unger, T. Porter, W. Culp, R. Labell, T. Matsunaga, R. Zutshi, Therapeutic applications of lipid-coated microbubbles, Adv. Drug Deliv. Rev. 56 (2004) 1291–1314.
[10] R.H. Abou-Saleh, M. Swain, S.D. Evans, N.H. Thomson, Poly(ethylene glycol) lipid-shelled microbubbles: abundance, stability, and mechanical properties, Langmuir 30 (2014) 5557–5563.
[11] M.A. Borden, G. Pu, G.J. Runner, M.L. Longo, Surface phase behavior and microstructure of lipid/PEG-emulsifier monolayer-coated microbubbles, Colloids Surf. B Biointerfaces 35 (2004) 209–223.
[12] J.N. Israelachvili, D.J. Mitchell, B.W. Ninham, Theory of self-assembly of hydrocarbon amphiphiles into micelles and bilayers, J. Chem. Soc. Faraday Trans. 2 (72) (1976) 1525–1568.
[13] M.M. Kozlov, D. Lichtenberg, D. Andelman, Shape of phospholipid/surfactant mixed micelles: cylinders or disks? Theoretical analysis, J. Phys. Chem. B 101 (1997) 6600–6606.
[14] A.K. Kenworthy, S.A. Simon, T.J. Mcintosh, Structure and phase-behavior of lipid suspensions containing phospholipids with covalently attached poly(Ethylene glycol), Biophys. J. 68 (1995) 1903–1920.
[15] K. Edwards, M. Johnsson, G. Karlsson, M. Silvander, Effect of polyethyleneglycol-phospholipids on aggregate structure in preparations of small unilamellar liposomes, Biophys. J. 73 (1997) 258–266.
[16] M.A. Borden, M.L. Longo, Dissolution behavior of lipid monolayer-coated, air-filled microbubbles: effect of lipid hydrophobic chain length, Langmuir 18 (2002) 9225–9233.
[17] G. Pu, M.A. Borden, M.L. Longo, Collapse and shedding transitions in binary lipid monolayers coating microbubbles, Langmuir 22 (2006) 2993–2999.
[18] J.J. Kwan, M.A. Borden, Microbubble dissolution in a multigas environment, Langmuir 26 (2010) 6542–6548.
[19] G. Pu, M.L. Longo, M.A. Borden, Effect of microstructure on molecular oxygen permeation through condensed phospholipid monolayers, J. Am. Chem. Soc. 127

(2005) 6524–6525.
[20] J.A. Feshitan, C.C. Chen, J.J. Kwan, M.A. Borden, Microbubble size isolation by differential centrifugation, J. Colloid Interface Sci. 329 (2009) 316–324.
[21] E.J. Swanson, V. Mohan, J. Kheir, M.A. Borden, Phospholipid-stabilized microbubble foam for injectable oxygen delivery, Langmuir 26 (2010) 15726–15729.
[22] D.J. Cox, J.L. Thomas, Ultrasound-induced dissolution of lipid-coated and uncoated gas bubbles, Langmuir 26 (2010) 14774–14781.
[23] M. Antonietti, S. Forster, Vesicles and liposomes: a self-assembly principle beyond lipids, Adv. Mater. 15 (2003) 1323–1333.
[24] H. Mulvana, E. Stride, J.V. Hajnal, R.J. Eckersley, Temperature dependent behavior of ultrasound contrast agents, Ultrasound Med. Biol. 36 (2010) 925–934.
[25] S. Garg, A.A. Thomas, M.A. Borden, The effect of lipid monolayer in-plane rigidity on in vivo microbubble circulation persistence, Biomaterials 34 (2013) 6862–6870.
[26] C.C. Chen, M.A. Borden, The role of poly(ethylene glycol) brush architecture in complement activation on targeted microbubble surfaces, Biomaterials 32 (2011) 6579–6587.
[27] M.A. Borden, M.L. Longo, The dependence of lipid-coated microbubble dissolution behavior on acyl chain length, Biophys. J. 82 (2002) 35a–35a.
[28] M.A. Borden, G. Pu, M.L. Longo, P.A. Dayton, K.W. Ferrara, Phase behavior and transport properties of the lipid-monolayer shell of a microbubble, Abstr. Pap. Am. Chem. S 230 (2005) U1072–U1073.
[29] S. Kilic, Quantification of PEG 40 St squeeze out from DSPC/PEG 40 St monolayers at higher molar ratios, Colloids Surf. A Physicochem. Eng. Asp. 551 (2018) 58–64.
[30] P. Wydro, K. Witkowska, The interactions between phosphatidylglycerol and phosphatidylethanolamines in model bacterial membranes:: the effect of the acyl chain length and saturation, Colloids Surf. B Biointerfaces 72 (2009) 32–39.
[31] F.J. Pavinatto, L. Caseli, A. Pavinatto, D.S. dos Santos Jr., T.M. Nobre, M.E.D. Zaniquelli, H.S. Silva, P.B. Miranda, O.N. de Oliveira Jr., Probing chitosan and phospholipid interactions using Langmuir and Langmuir-Blodgett films as cell membrane models, Langmuir 23 (2007) 7666–7671.
[32] P. Wydro, S. Knapczyk, M. Łapczyńska, Variations in the condensing effect of cholesterol on saturated versus unsaturated phosphatidylcholines at low and high sterol concentration, Langmuir 27 (9) (2011) 5433–5444.
[33] M.M. Lozano, M.L. Longo, Complex formation and other phase transformations mapped in saturated phosphatidylcholine/DSPE-PEG2000 monolayers, Soft Matter 5 (2009) 1822–1834.
[34] I. Kubo, S. Adachi, H. Maeda, A. Seki, Phosphatidylcholine monolayers observed with Brewster angle microscopy and π-A isotherms, Thin Solid Films 393 (2001) 80–85.
[35] K. Tanwir, V. Tsoukanova, Lateral distribution of a poly(ethylene glycol)-grafted phospholipid in phosphocholine monolayers studied by epifluorescence microscopy, Langmuir 24 (2008) 14078–14087.
[36] M.A. Borden, G. Pu, G.J. Runner, M.L. Longo, Surface phase behavior and microstructure of lipid/PEG-emulsifier monolayer-coated microbubbles, Colloids Surf. B Biointerfaces 35 (2004) 209–223.
[37] T.H. Chou, I. Chu, Thermodynamic characteristics of DSPC/DSPE-PEG2000 mixed monolayers on the water subphase at different temperatures, Colloids Surf. B Biointerfaces 27 (2003) 333–344.
[38] C.M. Hollinshead, R.D. Harvey, D.J. Barlow, J.R.P. Webster, A.V. Hughes, A. Weston, M.J. Lawrence, Effects of surface pressure on the structure of distearoylphosphatidylcholine monolayers formed at the air/water interface†, Langmuir 25 (2009) 4070–4077.
[39] Z. Xing, H. Ke, J. Wang, B. Zhao, X. Yue, Z. Dai, J. Liu, Novel ultrasound contrast agent based on microbubbles generated from surfactant mixtures of span 60 and polyoxyethylene 40 stearate, Acta Biomater. 6 (2010) 3542–3549.
[40] Y. Shen, R.L. Powell, M.L. Longo, Interfacial and stability study of microbubbles coated with a monostearin/monopalmitin-rich food emulsifier and PEG40 stearate, J. Colloid Interface Sci. 321 (2008) 186–194.
[41] Z.W. Xing, H.T. Ke, J.R. Wang, B. Zhao, X.L. Yue, Z.F. Dai, J.B. Liu, Novel ultrasound contrast agent based on microbubbles generated from surfactant mixtures of span 60 and polyoxyethylene 40 stearate, Acta Biomater. 6 (2010) 3542–3549.
[42] R.J. El-Khouri, S.L. Frey, A.W. Szmodis, E. Hall, K.J. Kauffman, T.E. Patten, K.Y.C. Lee, A.N. Parikh, A stripe-to-droplet transition driven by conformational transitions in a binary lipid-lipopolymer mixture at the air-water interface, Langmuir 27 (2011) 1900–1906.
[43] E. Aumaitre, D. Vella, P. Cicuta, On the measurement of the surface pressure in Langmuir films with finite shear elasticity, Soft Matter 7 (2011) 2530–2537.
[44] T.R. Baekmark, G. Elender, D.D. Lasic, E. Sackmann, Conformational transitions of mixed monolayers of phospholipids and polyethylene oxide lipopolymers and interaction forces with solid surfaces, Langmuir 11 (1995) 3975–3987.
[45] S. Nakamura, H. Nakahara, M.P. Krafft, O. Shibata, Two-component Langmuir monolayers of single-chain partially fluorinated amphiphiles with dipalmitoylphosphatidylcholine (DPPC), Langmuir 23 (2007) 12634–12644.
[46] J. Minones, J. Rodríguez Patino, O. Conde, C. Carrera, R. Seoane, The effect of polar groups on structural characteristics of phospholipid monolayers spread at the air-water interface, Colloids Surf. A Physicochem. Eng. Asp. 203 (2002) 273–286.
[47] H. Nakahara, M.P. Krafft, A. Shibata, O. Shibata, Interaction of a partially fluorinated alcohol (F8H11OH) with biomembrane constituents in two-component monolayers, Soft Matter 7 (2011) 7325–7333.
[48] J.M.R. Patino, C.C. Sanchez, M.R.R. Nino, Morphological and structural characteristics of monoglyceride monolayers at the air-water interface observed by Brewster angle microscopy, Langmuir 15 (1999) 2484–2492.
[49] M.N.G. de Mul, J.A. Mann, Determination of the thickness and optical properties of a Langmuir film from the domain morphology by Brewster angle microscopy, Langmuir 14 (1998) 2455–2466.
[50] K. Winsel, D. Honig, K. Lunkenheimer, K. Geggel, C. Witt, Quantitative Brewster angle microscopy of the surface film of human broncho-alveolar lavage fluid, Eur. Biophys. J. Biophys. 32 (2003) 544–552.
[51] O. Tirosh, Y. Barenholz, J. Katzhendler, A. Priev, Hydration of polyethylene glycol-grafted liposomes, Biophys. J. 74 (1998) 1371–1379.
[52] F. Albertorio, A.J. Diaz, T.L. Yang, V.A. Chapa, S. Kataoka, E.T. Castellana, P.S. Cremer, Fluid and air-stable lipopolymer membranes for biosensor applications, Langmuir 21 (2005) 7476–7482.
[53] M.A. Borden, G.V. Martinez, J. Ricker, N. Tsvetkova, M. Longo, R.J. Gillies, P.A. Dayton, K.W. Ferrara, Lateral phase separation in lipid-coated microbubbles, Langmuir 22 (2006) 4291–4297.
[54] M.A. Borden, Microbubble dispersions of natural lung surfactant, Curr. Opin. Colloid Interface Sci. 19 (2014) 480–489.
[55] A. Gopal, K.Y.C. Lee, Morphology and collapse transitions in binary phospholipid monolayers, J. Phys. Chem. B 105 (2001) 10348–10354.
[56] C. Ybert, W.X. Lu, G. Moller, C.M. Knobler, Collapse of a monolayer by three mechanisms, J. Phys. Chem. B 106 (2002) 2004–2008.
[57] M. Lipp, K. Lee, D. Takamoto, J. Zasadzinski, A. Waring, Coexistence of buckled and flat monolayers, Phys. Rev. Lett. 81 (1998) 1650–1653.
[58] Avanti, March (2018).
[59] Sigma-Aldrich, March (2018).